Induced pluripotent stem cell-based disease modeling identifies ligand-induced decay of megalin as a cause of Donnai-Barrow syndrome

see commentary on page 54

Julia Flemming[1,5], Maike Marczenke[1,5], Ina-Maria Rudolph[1], Rikke Nielsen[2], Tina Storm[2], Ilsoe Christensen Erik[2], Sebastian Diecke[1], Francesco Emma[3] and Thomas E. Willnow[1,2]

[1]Max-Delbrueck-Center for Molecular Medicine, Berlin, Germany; [2]Department of Biomedicine, Faculty of Health Science, Aarhus University, Aarhus C, Denmark; and [3]Division of Nephrology, Department of Pediatric Subspecialties, Bambino Gesù Children's Hospital – IRCCS, Rome, Italy

Donnai-Barrow syndrome (DBS) is an autosomal-recessive disorder characterized by multiple pathologies including malformation of forebrain and eyes, as well as resorption defects of the kidney proximal tubule. The underlying cause of DBS are mutations in *LRP2*, encoding the multifunctional endocytic receptor megalin. Here, we identified a unique missense mutation R3192Q of *LRP2* in an affected family that may provide novel insights into the molecular causes of receptor dysfunction in the kidney proximal tubule and other tissues affected in DBS. Using patient-derived induced pluripotent stem cell lines we generated neuroepithelial and kidney cell types as models of the disease. Using these cell models, we documented the inability of megalin R3192Q to properly discharge ligand and ligand-induced receptor decay in lysosomes. Thus, mutant receptors are aberrantly targeted to lysosomes for catabolism, essentially depleting megalin in the presence of ligand in this affected family.

Kidney International (2020) **98,** 159–167; https://doi.org/10.1016/j.kint.2020.02.021

KEYWORDS: endocytosis; low-molecular-weight proteinuria; proximal tubule dysfunction; renal Fanconi syndrome

Correspondence: *Thomas E. Willnow, Max-Delbrueck-Center for Molecular Medicine, Robert-Roessle-Str. 10, D-13125 Berlin, Germany. E-mail: willnow@mdc-berlin.de*

[5]These authors contributed equally to the study.

Received 29 May 2019; revised 11 February 2020; accepted 13 February 2020; published online 24 March 2020

Donnai-Barrow/Facio-oculo-acoustico-renal syndrome (herein referred to as DBS) is an autosomal recessive disorder caused by inheritable mutations in *LRP2* (low-density lipoprotein receptor–related protein 2).[1,2] This gene encodes the endocytic receptor megalin that acts as a high-capacity clearance pathway for numerous ligands in absorptive epithelia, most notably in the developing forebrain and retina[3-5] and in the proximal tubules of the adult kidney.[6,7] Some variability exists in the extent of malformation of forebrain and facial structures in patients with DBS, defects attributed to the loss of receptor expression in neuroepithelial cells of the developing central nervous system.[2,8-10] By contrast, patients with DBS invariably suffer from renal resorption defects (renal Fanconi syndrome) characterized by urinary loss of megalin ligands, including vitamins D, A, and B12 bound to their plasma carrier proteins.[1,11,12] This observation underscores the central role played by megalin in proximal tubular retrieval processes in humans.

Despite its importance for renal (patho)physiology, little is known about the functional organization of the giant 600 kDa receptor megalin and the molecular mechanisms that define its ability to act as a clearance pathway in the kidney and other tissues of the human body. Naturally occurring mutations in DBS may shed light on essential protein domains altered in the mutant receptors. However, most known *LRP2* mutations encode truncated soluble fragments offering little conceptual advance on the functional organization of the receptor polypeptide.[1] Here, we report the identification of a novel missense mutation $LRP2^{R3192Q}$ in 2 siblings with DBS. Using human disease modeling in neuroepithelial and renal cell types generated from induced pluripotent stem cells (iPSCs) of both individuals, we document that mutation $LRP2^{R3192Q}$ disrupts the ability of megalin to properly discharge internalized ligand. As a consequence, mutant receptors are aberrantly targeted to lysosomes for catabolism, essentially depleting DBS cells for megalin in the presence of ligand.

RESULTS

iPSC-derived cell lines for disease modeling of DBS

We identified 2 siblings who presented with clinical symptoms of renal Fanconi syndrome, including hypercalciuria and abnormal urinary excretion of low-molecular-weight

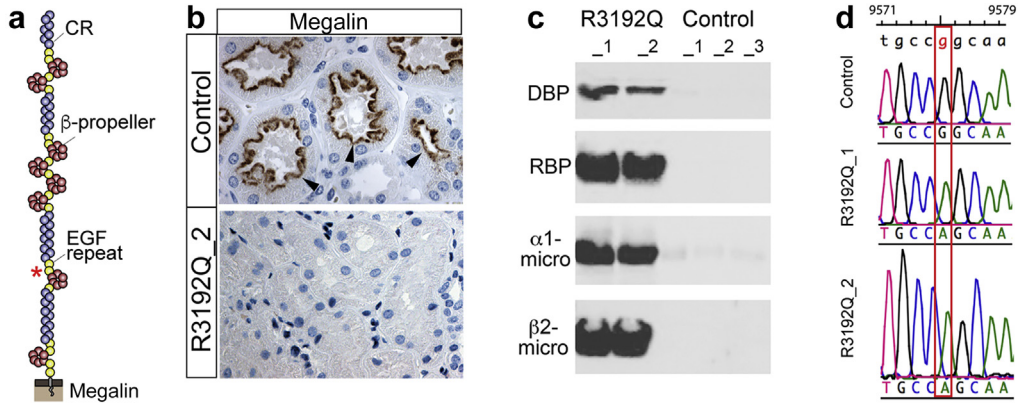

Figure 1 | Mutation c:G9575A in Donnai-Barrow syndrome disrupts renal megalin^{R3192Q} expression. (**a**) Structural organization of the megalin polypeptide composed of complement-type repeats (CR), epidermal growth factor (EGF)–type repeats, and β-propellers. Mutation R3192Q (encoded by c:G9575A) in an EGF-type repeat is indicated by the red asterisk. (**b**) Immunohistological detection of megalin (arrowheads) in proximal tubule cells of kidney biopsies from a control subject but not from patient R3192Q_2. (**c**) Western blot analysis of spot urine documenting urinary loss of the megalin ligands vitamin D–binding protein (DBP), retinol-binding protein (RBP), α_1-microglobulin, and β_2-microglobulin in patients R3192Q_1 and R3192Q_2, but not in 3 control subjects. (**d**) Sequence analysis showing a homozygous mutation c:G9575A (red box) in *LRP2* in induced pluripotent stem cell lines derived from patients R3192Q_1 and R3192Q_2 as compared with a control cell line. Sequences were aligned to the *LRP2* reference sequence given above (NCBI reference sequence: NM_004525.2). To optimize viewing of this image, please see the online version of this article at www.kidney-international.org.

proteins at the age of 7 and 9, respectively (see the Patient information section for more clinical details). Exome sequencing identified homozygosity for mutation c:G9575A in *LRP2* in both individuals, resulting in amino acid alteration R3192Q in an epidermal growth factor–type repeat in the extracellular megalin domain (Figure 1a). Megalin deficiency as the underlying cause of renal Fanconi syndrome was confirmed by the absence of receptor expression in renal biopsies (Figure 1b) and by aberrant urinary excretion of known receptor ligands (Figure 1c) in the affected individuals R3192Q_1 and R3192Q_2.

To elucidate the mechanism impairing megalin^{R3192Q} expression, we generated iPSC lines by reprogramming peripheral blood mononuclear cells from both patients. Homozygosity for c:G9575A in the iPSC lines was confirmed by DNA sequencing (Figure 1d). Karyotyping of peripheral blood mononuclear cells, and iPSC lines derived thereof, identified copy neutral loss of heterozygosity at 2q23.3-q31.1 as the reason for homozygosity for c:G9575A (Supplementary Figure S1A and B). Minor alterations in other chromosomal regions common to peripheral blood mononuclear cells and iPSC lines were considered irrelevant to explain the loss of renal megalin expression in the affected individuals (Supplementary Figure S1C and D).

iPSC lines from patients R3192Q_1 and R3192Q_2 showed robust expression of pluripotency markers (Supplementary Figure S2A and B) and the expected potential to differentiate into all 3 germ layers (Supplementary Figure S2C and D). To derive a cell model for studying the molecular mechanism underlying loss of megalin^{R3192Q} expression, we initially applied a protocol whereby iPSCs were differentiated into neural precursor cells (NPCs), the progenitor cell population for various cell types of the developing central nervous system (Supplementary Figure S3A).[13] We chose this differentiation protocol for our initial studies because of its robustness and reproducibility, and because it recapitulates expression of megalin in this cell type *in vivo*.[4,14] Both patient cell lines faithfully recapitulated neuroectodermal differentiation as exemplified by induction of neuroectodermal markers PAX6 and SOX1, and by a concomitant loss of pluripotency marker OCT4 (Supplementary Figure S3B–E).

When expression of megalin during neuroectodermal differentiation was tested by immunocytochemistry, robust induction of receptor levels was seen in R3192Q_1 and control cell lines at day 5 of differentiation (Figure 2a). However, megalin levels decreased significantly by day 9 in patient as compared with control cells (Figure 2a). Loss of megalin^{R3192Q} at later stages of differentiation was not due to a decrease in gene transcription, as *LRP2* transcript levels were similar to control cells at days 5 and 9 of differentiation (Figure 2b). The reduced level of megalin protein, but not transcript at day 9 of differentiation, was substantiated by Western blot (Figure 2c and d) and quantitative real-time polymerase chain reaction analysis (Figure 2e), respectively. Post-transcriptional loss of megalin expression was reproduced in an iPSC line from patient R3192Q_2 using immunocytochemistry and quantitative real-time polymerase chain reaction (Supplementary Figure S4A, B, and E), as well as Western blotting (Supplementary Figure S4C and D).

Mutation R3192Q does not abolish the endocytic activity of megalin

To interrogate the impact of mutation R3192Q on the activity of megalin, we established an endocytosis assay in NPCs using the amino terminal fragment of sonic hedgehog (SHH-N) fused to glutathione S-transferase, a megalin ligand in several

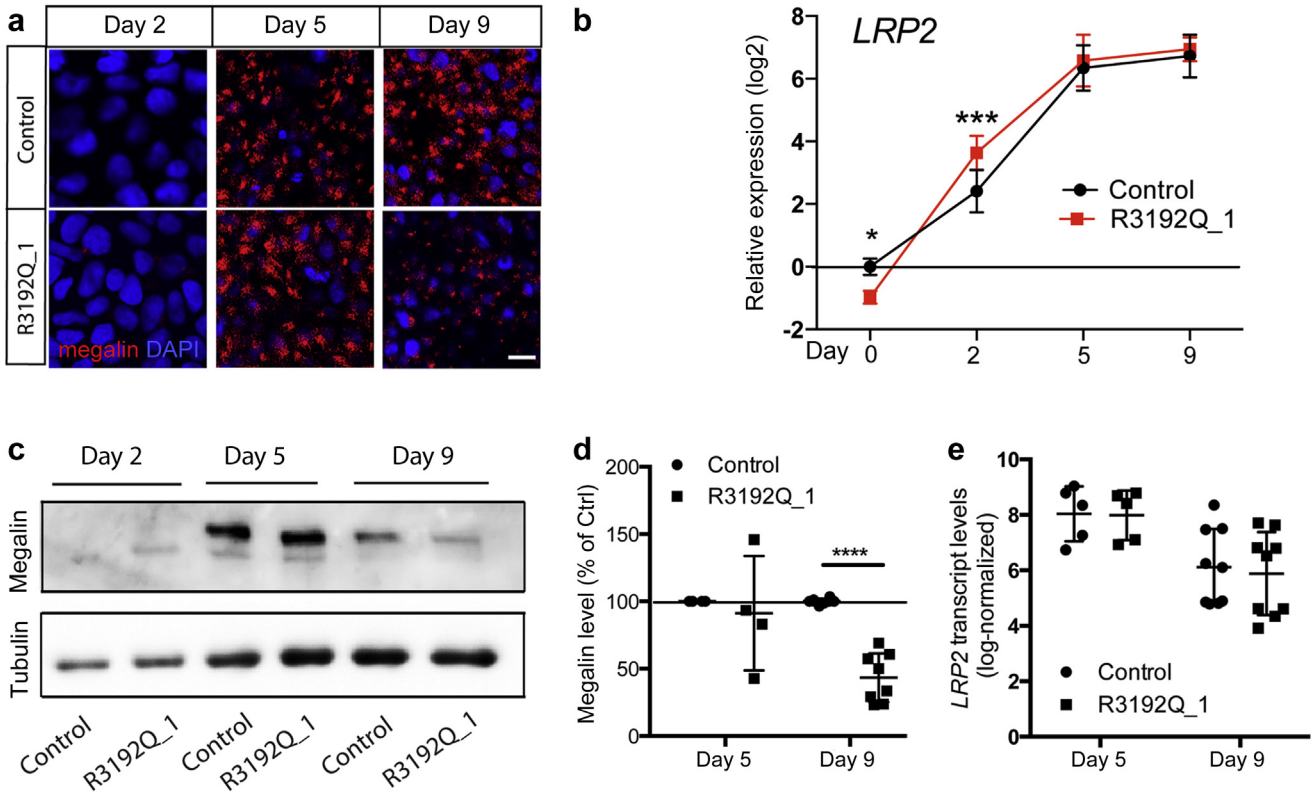

Figure 2 | Cellular expression of megalin^{R3192Q} is impacted by a post-transcriptional mechanism. (**a**) Immunodetection of megalin (red) in induced pluripotent stem cell (iPSC) lines at the indicated time points of neuroectodermal differentiation. Cells were counterstained with 4′,6-diamidino-2-phenylindole (DAPI) (blue). Megalin expression was induced from day 5 onward in both genotypes. At day 9, receptor levels decreased in patient-derived cells as compared with control cells. Bar = 10 μm. (**b**) Transcript levels of *LRP2* during differentiation into neuroectoderm cells in the control subject and patient R3192Q_1. Data are depicted as Δct normalized to day 0 of the control cells (ΔΔct) ± SD; n = 4 experiments with 2–3 biological replicates/experiment. Statistical analyses were performed by 2-way analysis of variance with the Bonferroni post-test. *$P < 0.05$; ***$P < 0.001$. (**c**) Western blot analysis of megalin in R3192Q_1 and control iPSC lines at the indicated time points of neuroectodermal differentiation. The detection of α-tubulin served as loading control. (**d**) Megalin levels were quantified by densitometric scanning of replicate Western blots (exemplified in panel **c**) in control and R3192Q_1 neural precursor cells (NPCs) at days 5 and 9 of differentiation (n = 2–3 independent experiments, 2–4 biological replicates/experiment). Megalin levels in R3192Q_1 cells were comparable with control cells at day 5, but significantly decreased at day 9 of differentiation. Values are given as relative levels of expression compared with controls (set to 100% ± SD). Statistical significance was determined by Student's *t* test (day 9) or 1-paired *t* test (day 5). ****$P < 0.0001$. (**e**) Quantitative real-time polymerase chain reaction analysis of *LRP2* transcript levels in a control and R3192Q_1 NPCs at days 5 and 9 of differentiation. (n = 3 independent experiments, 2–4 biological replicates/experiment). Levels are depicted as ct values normalized to transcript levels of *GAPDH* (Δct ± SD) used as an internal control. Transcript levels for *LRP2* are unchanged at days 5 and 9 comparing genotypes (Student's *t* test). To optimize viewing of this image, please see the online version of this article at www.kidney-international.org.

tissues.[4,15] To first establish the validity of this assay for scoring megalin activity, we used a CRISPR/Cas9 strategy to disrupt the megalin coding sequence in the control cell line used in this study and to generate a cell clone genetically deficient for this receptor ($LRP2^{-/-}$; Supplementary Figure S5A). Deletion of the ATG codon in the *LRP2* gene locus completely ablated megalin expression in this cell clone as shown by Western blot analysis (Supplementary Figure S5B). The absence of megalin severely reduced the uptake of GST-SHH-N in $LRP2^{-/-}$ NPCs as compared with parental cells ($LRP2^{+/+}$) as documented by immunocytochemistry (Supplementary Figure S5C), identifying megalin as the major endocytic route for SHH-N in NPCs. To more accurately assess the quantitative contribution of megalin to SHH-N uptake in these cells, we treated $LRP2^{-/-}$ and control NPCs with GST-SHH-N and determined the amount of cell-associated ligand thereafter using Western blotting (Supplementary Figure S5B). Megalin deficiency reduced the amount of GST-SHH-N in the $LRP2^{-/-}$ cell fraction by 50% as compared with control cells, underscoring the significance of megalin as the SHH receptor in NPCs (Supplementary Figure S5D). The residual amount of GST-SHH-N associated with $LRP2^{-/-}$ NPCs likely reflected adherence of the ligand to the cellular surface, although the existence of other uptake mechanisms, such as through the receptor Patched1, cannot be excluded.

Next, we used the GST-SHH-N uptake assay to assess the receptor activity in the patient cell line R3192Q_1. Ligand uptake was reduced in these cells as compared with control NPCs as documented by immunocytochemistry (Figure 3a) and quantitative Western blotting (Figure 3b and c). Still, the megalin-mediated uptake of GST-SHH-N in the cell line

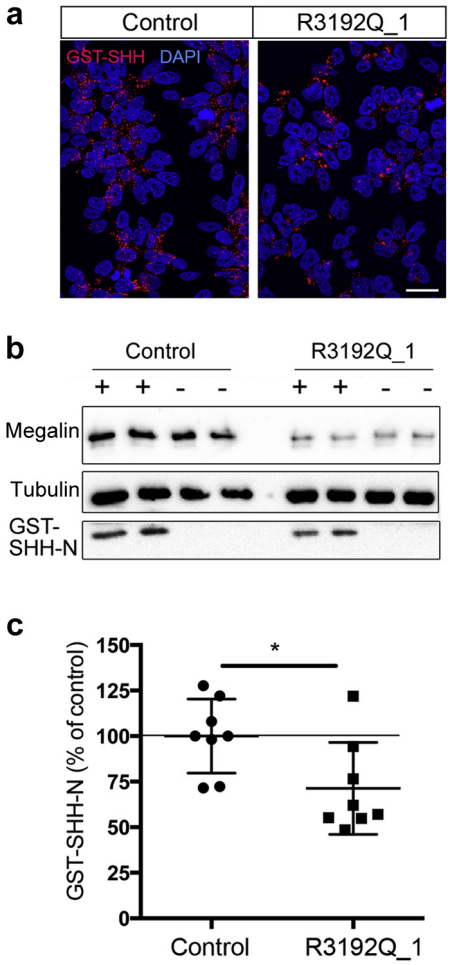

Figure 3 | Mutation c:G9575A does not impact the endocytic activity of megalin^{R3192Q}. (**a**) Neural precursor cells (NPCs) from a control or from patient R3192Q_1 were treated for 2 hours in medium containing 10 μg/ml recombinant GST-SHH-N. Subsequently, cells were immunostained for GST-SHH-N (red) using anti-GST antisera and counterstained with 4′,6-diamidino-2-phenylindole (DAPI) (blue). Bar = 25 μm. (**b**) NPCs from a control or from patient R3192Q_1 at day 9 of differentiation were treated overnight in medium with (+) or without (−) 10 μg/ml recombinant GST-SHH-N. Thereafter, levels of megalin and GST-SHH-N in cell extracts were determined by Western blotting. Detection of α-tubulin served as loading control. (**c**) Quantification of GST-SHH-N uptake in control and R3192Q_1 cells by densitometric scanning of replicate Western blots (exemplified in panel **b**). Levels are given relative to control cells (set to 100% ± SD). The amount of internalized GST-SHH-N is significantly lower in cells from patients R3192Q_1 as compared with control cells (n = 3 independent experiments, 2–4 biological replicates/experiment; Student's *t* test). *$P < 0.05$. To optimize viewing of this image, please see the online version of this article at www.kidney-international.org.

R3192Q_1 was apparent and substantially higher than in receptor null cells (75% of control in Figure 3c vs. 50% of control in Supplementary Figure S5D). These findings indicated that impaired expression of megalin^{R3192Q} reduced but did not abolish the ability of NPCs to internalize receptor ligands.

SHH induces loss of megalin^{R3192Q} expression in neuroepithelial and renal cell types

Our data revealed the surprising finding that mutation R3192Q did not ablate expression or endocytic activity of megalin but impacted receptor levels by a post-transcriptional mechanism. As our differentiation protocol entailed the addition of SHH at day 5 of differentiation (Supplementary Figure S3A), we reasoned that this ligand may trigger the decline in megalin^{R3192Q} levels seen at day 9. To test this hypothesis, we used NPCs at day 5 of differentiation and incubated them with or without GST-SHH-N. The addition of ligand resulted in significantly lower megalin levels in the patient cell line R3192Q_1 (Figure 4a and b) as compared with the untreated cells. Similarly, levels of mutant megalin were also decreased on ligand exposure in the patient cell line R3192Q_2, although an increase in wild-type receptor contributed to the difference in megalin levels seen between patient 2 and control cells (Supplementary Figure S6A and B). Decreased levels of megalin^{R3192Q} in the presence of GST-SHH-N were due to a reduced half-life of the mutant receptor as shown by determining protein stability in NPCs treated with cycloheximide, an inhibitor of protein translation (Figure 4c and d).

To substantiate that ligand-induced decay of megalin^{R3192Q} was also seen in renal cell types and potentially responsible for renal Fanconi syndrome in affected individuals, we applied an established protocol to differentiate iPSCs into renal proximal tubule epithelial-like cells (RPTECs)[16] (Supplementary Figure S7A). Differentiation into the proper renal cell type was documented by transient expression of mesodermal marker *T/Brachyury* and early proximal renal vesicle marker *JAG1*, as well as by stable induction of proximal tubule markers *AQP1* and *LRP2* (Supplementary Figure S7B). Coexpression of AQP1 and megalin in the differentiated cells was substantiated by immunocytochemistry (Supplementary Figure S7C). As shown for NPCs above, the addition of GST-SHH-N resulted in lower megalin levels in R3192Q_1 as compared with control cells (Figure 5a and b). To query whether other receptor ligands may also impact expression of megalin^{R3192Q} in RPTECs, we tested the effect of lysozyme, a protein cleared from the glomerular filtrate by megalin.[17] Contrary to SHH-N, the addition of lysozyme to the cell medium did not impact levels of megalin^{R3192Q} (Supplementary Figure S8).

Aberrant lysosomal targeting of receptor/SHH complexes induces catabolism of megalin^{R3192Q}

To explore the reasons for the reduced stability of megalin^{R3192Q} in the presence of GST-SHH-N, we studied the subcellular localization of the receptor and ligand. When the subcellular localizations of megalin and internalized GST-SHH-N were tested by immunocytochemistry in NPCs, an increased colocalization of megalin^{R3192Q} with this ligand was observed in both patients' cell lines as compared with the wild-type receptor (Figure 6a and b; Supplementary Figure S9A and B). As shown by co-

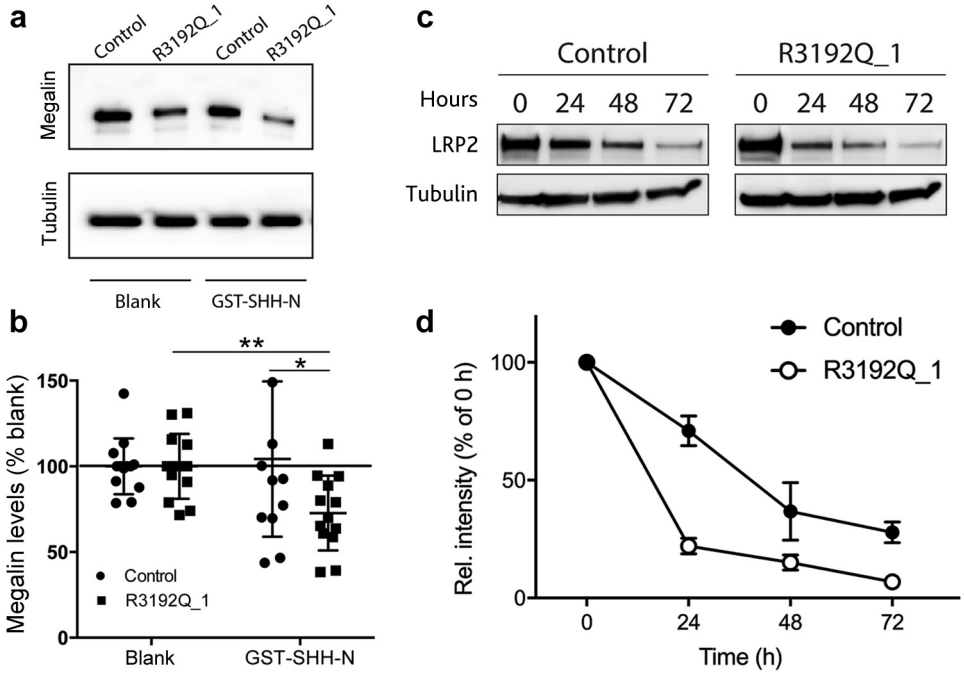

Figure 4 | The addition of SHH-N decreases stability of megalin^{R3192Q} in neural precursor cells (NPCs). (**a**) NPCs at day 5 of differentiation were treated with 10 μg/ml GST-SHH-N or blank medium overnight, and levels of megalin were determined in cell lysates by Western blotting thereafter. Detection of α-tubulin served as a loading control. (**b**) Quantification of megalin levels in control and R3192Q_1 NPC lines by densitometric scanning of replicate Western blots (exemplified in panel **a**). Levels are given as relative to the untreated condition (set to 100% ± SD). In the presence of GST-SHH-N, levels of megalin^{R3192Q} were significantly lower compared with that of the wild-type receptor (n = 4 independent experiments, 2–3 biological replicates/experiment). This difference was not seen in the control medium (blank) lacking the receptor ligand. Statistical significance was determined using Student's *t* test. *$P < 0.05$; **$P < 0.01$. (**c**) Replicate layers of control and R3192Q_1 NPCs at day 5 of differentiation were treated with 10 μg/ml GST-SHH-N and 7.5 μg/ml cycloheximide. Cells were harvested at the indicated time points, and expression levels of megalin were determined by Western blotting. Detection of α-tubulin served as a loading control. (**d**) Megalin levels were quantified by densitometric scanning of replicate Western blots (exemplified in panel **c**) in control and R3192Q_1 NPCs after treatment with GST-SHH-N and cycloheximide (mean of 3 independent experiments). Receptor levels are given as a percentage of levels at time point 0 of treatment for each cell line. In the presence of a ligand, a significantly faster decay was observed for megalin^{R3192Q} as compared with the wild-type receptor ($P < 0.0001$ for genotype and time, unmatched 2-way analysis of variance).

immunostaining with lysosomal marker LAMP1, the addition of ligand provided a protective effect to wild-type megalin reducing its localization to LAMP1+ lysosomes. This protective effect was not seen with megalin^{R3192Q}, resulting in enhanced lysosomal trapping in the presence of ligand as compared with the wild-type receptor (Figure 6c and d; Supplementary Figure S9C and D). No difference in lysosomal targeting of megalin was seen between mutant and control cells when treated with GST only (Figure 6c and d; Supplementary Figure S9C and D). Triple immunostaining substantiated enhanced colocalization of megalin^{R3192Q} and GST-SHH-N in LAMP1+ lysosomes (Figure 6e).

To further corroborate ligand-induced lysosomal catabolism of megalin^{R3192Q} as a molecular cause of DBS, we treated control and mutant NPCs with GST-SHH-N in the presence or absence of lysosomal inhibitors. Lysosomal blockade did not alter the levels of wild-type megalin, but it significantly increased levels of the mutant receptor (Figure 7). These findings further substantiated that lysosomal degradation significantly contributes to the reduced stability of megalin^{R3192Q} in DBS.

DISCUSSION

Megalin is the main endocytic receptor in the proximal convoluted tubules for bulk clearance of plasma proteins from the glomerular filtrate.[6,7,17,18] Megalin-mediated clearance of ligands has also been shown in other absorptive epithelia, including the neural tube,[4] the epididymis,[19] and the retinal pigment epithelium.[5] So far, the inability to recombinantly express full-length megalin has hampered attempts to dissect functional domains in the receptor polypeptide. Now, the availability of naturally occurring *LRP2* mutations in patients with DBS and the ability to recapitulate mutant phenotypes in iPSC-derived cell models significantly advance our abilities to study megalin in human health and disease. This assumption is substantiated by our studies of individuals homozygous for a novel *LRP2* mutation c:G9575A. Based on the absence of megalin in renal biopsies (Figure 1b), the inability to properly fold and express megalin^{R3192Q} may have been anticipated as a consequence of this mutation. However, studies in iPSC-derived cell lines document proper expression of the mutant receptor in the absence of ligands in neuroepithelial (Figure 2a and Supplementary Figure S4A) and proximal tubule (Supplementary

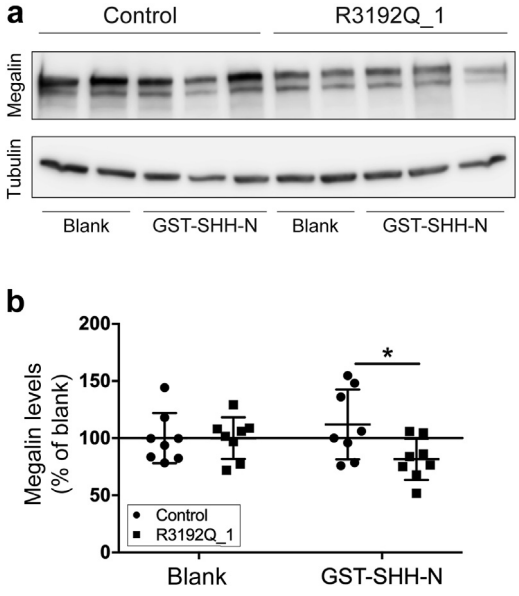

Figure 5 | Ligand-induced decay of megalin^{R3192Q} in induced pluripotent stem cell (iPSC)–derived renal proximal tubule epithelial-like cells (RPTECs). (**a**) Control and patient iPSC-derived RPTECs at day 8 of differentiation were treated with 10 μg/ml GST-SHH-N or blank (10 μg/ml GST) medium overnight. Subsequently, megalin levels in cell lysates were determined by Western blotting. Detection of α-tubulin served as a loading control. (**b**) Megalin levels in a control and R3192Q_1 RPTECs were quantified by densitometric scanning of replicate Western blots (exemplified in panel **a**). Levels are given as relative to the untreated condition (set at 100% ± SD). In the presence of GST-SHH-N, levels of megalin^{R3192Q} were significantly lower as compared with the wild-type receptor (n = 3 independent experiments, 2–3 biological replicates/experiment). Statistical significance was determined using Student's *t* test. *$P < 0.05$.

Figure S7C) cell types. Also, the ability to perform endocytosis does not seem to be overtly impacted as judged from the ability of the mutant receptor to clear the ligands SHH-N (Figure 3) and lysozyme (Supplementary Figure S8). Rather, extended retention of receptor/ligand complexes (Figure 6a and b; Supplementary Figure S9AB and B) and enhanced accumulation of the receptor to lysosomal compartments in the presence of ligands (Figure 6c–e; Supplementary Figure S9C and D) argue for the induced decay of megalin^{R3192Q} because of an inability to properly discharge some ligands in the endocytic pathway. Blockade of lysosomal activity significantly increases levels of megalin^{R3192Q} but not of the wild-type receptor (Figure 7). This finding supports targeting to lysosomes as a factor that specifically contributes to the impaired stability of the mutant receptor in neuroepithelial and renal cells types. Remarkably, a similar mechanism has been identified as a cause of low-density lipoprotein receptor deficiency in familial hypercholesterolemia (class 5 mutations).[20] Our hypothesis is backed by the localization of R3192Q in an epidermal growth factor–type repeat, a domain required for endosomal discharge of ligands by the low-density lipoprotein receptor.[21]

Much of our cell biological studies have focused on the interaction of megalin with its ligand SHH-N in NPCs, an interaction considered crucial to the role of this receptor in the development of forebrain and eyes.[3,4] Individuals homozygous for *LRP2*^{R3192Q} do not present with obvious craniofacial malformations, recapitulating earlier observations that missense mutations in *LRP2* feature mild forms or even the absence of forebrain anomalies.[8,9] However, both individuals present with severe myopia (+7 and +9 dioptres, respectively), indicating massive overgrowth of the eyes as a consequence of potentially impaired uptake of SHH-N[3] and other megalin ligands[5] in the retinal pigment epithelium. Although aberrant targeting of megalin^{R3192Q} to lysosomes has only been shown directly in NPCs, the ability of SHH-N to induce the decay of the mutant receptor in iPSC-derived RPTECs strongly argues that a similar disease mechanism is operable in the kidney and responsible for renal Fanconi syndrome in this family with DBS.

As megalin acts as a high-capacity clearance receptor for numerous ligands in the renal proximal tubule, the question remains whether only SHH-N or also other receptor ligands destine megalin^{R3192Q} to lysosomal catabolism. Conceivably, the induced decay of the mutant receptor may be caused by ligands, which binding sites are altered by c:G9575A, but not by others not impacted by this mutation. In our hands, lysozyme did not decrease the stability of the mutant receptor in RPTECs (Supplementary Figure S8), documenting that the proposed disease mechanism is not applicable to every ligand. Unfortunately, little is known about the exact binding sites for SHH, lysozyme, or most other receptor ligands that may guide our choice of alternative ligands to be tested. Still, irrespective of the number of ligands that may cause the lysosomal decay of megalin^{R3192Q}, our findings highlight an important new concept in receptor cell biology, relevant for pathophysiology of the kidney and other tissues that require the endocytic activity of megalin.

METHODS

Patient information

The patients are son and daughter of apparently unrelated parents originating from the same small town in Italy. They were diagnosed with proteinuria when aged 7 and 9 years, respectively. The brother presented first, after discovering proteinuria in a spot urine analysis (30 mg/dl) performed during a varicella zoster infection. Further investigations revealed mild kidney insufficiency (estimated glomerular filtration rate: 86 ml/min per 1.73 m^2), increased urinary protein/creatinine ratio (1.35 mg/mg [n.v. < 0.2 mg/mg]), hypercalciuria (urinary calcium/creatinine ratio: 0.31 mg/mg [n.v. < 0.2 mg/mg]), and abnormal urinary excretion of low-molecular-weight proteins (urinary beta 2 microglobulin/creatinine ratio: 0.48 mg/mg [n.v. absent]). Other tests showed normal serum bicarbonate levels, normal renal phosphate handling (serum phosphate: 5.1 mg/dl [n.v. > 3.5 mg/dl]; TmP/GFR: 4.2 mg/dl [n.v. > 2.9 mg/dl]), and normal excretion of amino acids, glucose, uric acid, sodium, and magnesium. The urine sediment was normal. Renal ultrasound showed normal sized kidneys (approximately 10th percentile), with very mild hyperechogenicity. The physical examination was unremarkable, except for

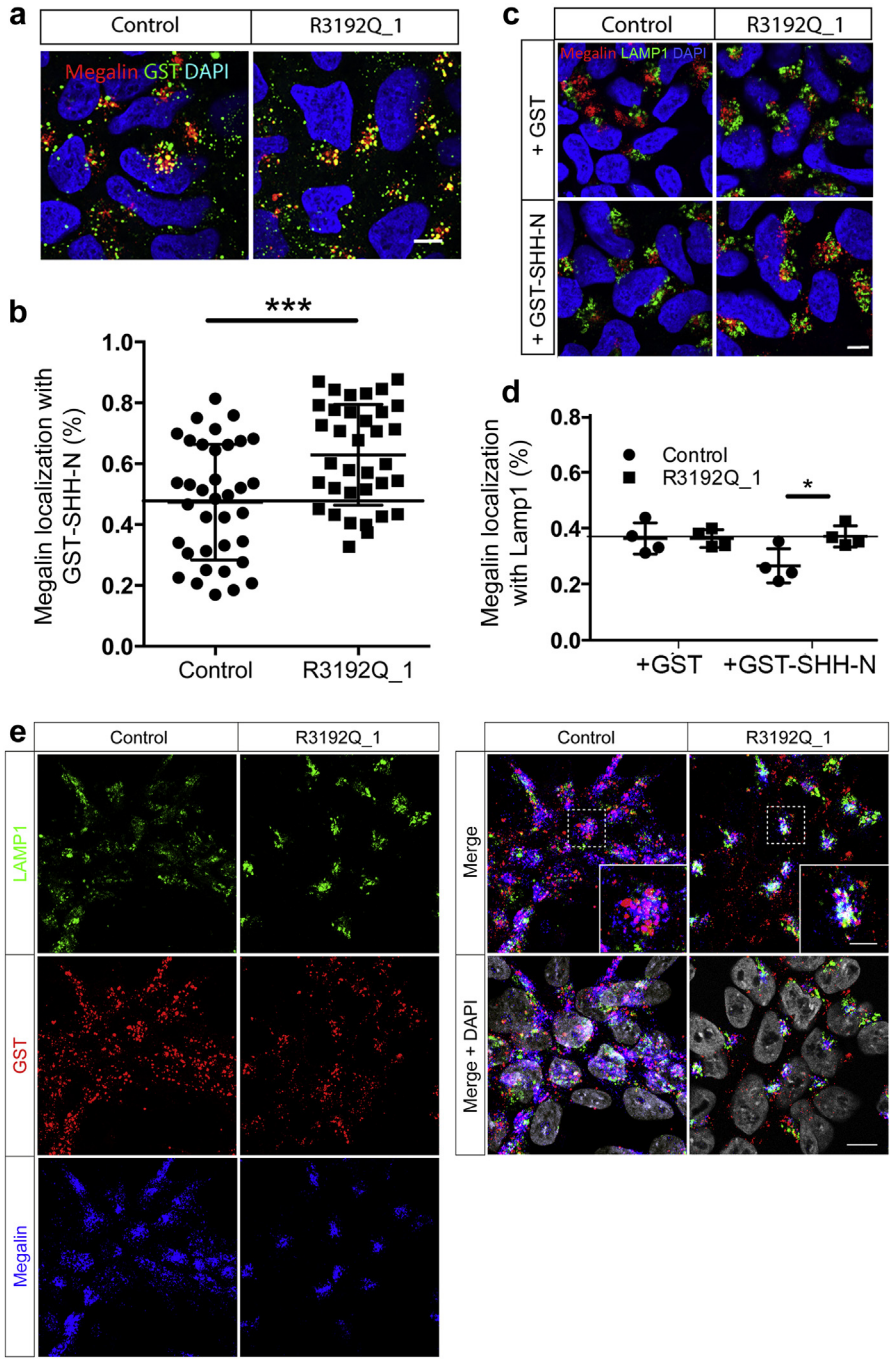

Figure 6 | Binding of GST-SHH-N directs megalin^{R3192Q} to lysosomes. (**a**) Immunofluorescence detection of megalin (red) and GST-SHH-N (green) in control and patient neural precursor cells (NPCs) at day 7 of differentiation treated with 10 μg/ml GST-SHH-N for 2 hours. Cells were counterstained with 4′,6-diamidino-2-phenylindole (DAPI) (blue). Bar = 8 μm. (**b**) Extent of colocalization of megalin with GST-SHH-N as determined by Mander's colocalization coefficient is increased for megalin^{R3192Q} as compared with wild-type megalin, suggesting the prolonged interaction of the mutant receptor with its ligand. One representative experiment is shown with data given as mean ± SD. This experiment was repeated 4 times with 25–40 cells/experiment analyzed. All 4 experiments showed statistical significance (Student's *t* test). ***$P < 0.0001$. (**c**) Immunofluorescence detection of megalin (red) and lysosomal marker LAMP1 (green) in control and patient NPCs at day 7 of differentiation treated with 10 μg/ml GST or GST-SHH-N for 2 hours. Cells were counterstained with DAPI. Bar = 8 μm. (**d**) Mander's colocalization coefficient documents increased colocalization of megalin^{R3192Q} with LAMP1 in NPCs treated with GST-SHH-N (but not GST) as compared with wild-type megalin (n = mean of 4 experiments with 15–40 cells/experiment analyzed ± SD; Student's *t* test). (**e**) Immunodetection of lysosomal marker LAMP1 (green), GST-SHH-N (red), and megalin (blue) in control and patient NPCs at day 7 of differentiation. Cells were treated with 10 μg/ml GST-SHH-N for 2 hours and counterstained with DAPI (gray). Bar = 10 μm. Higher magnifications of overview pictures are given as insets (bars = 4 μm). Increased colocalization of megalin with GST-SHH-N in LAMP1+ lysosomal vesicles (white signals) was noted in patient as compared with control NPC lines. To optimize viewing of this image, please see the online version of this article at www.kidney-international.org.

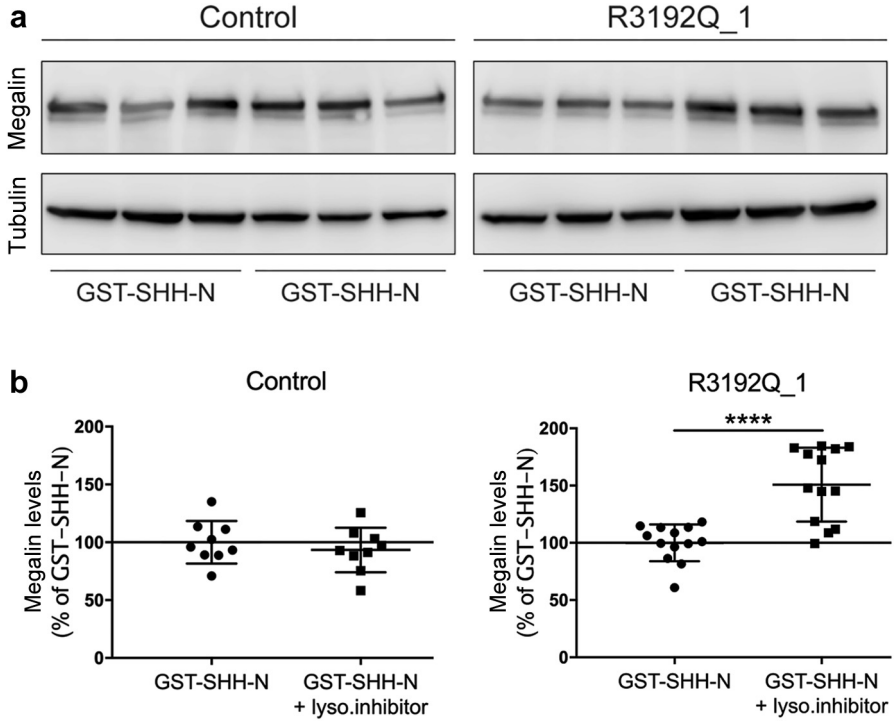

Figure 7 | Inhibition of lysosomal proteases prevents the ligand-induced decay of megalin^{R3192Q}. (**a**) Neural precursor cells (NPCs) at differentiation day 5 were treated overnight with 10 μg/ml GST-SHH-N in the absence or presence of lysosomal protease inhibitors (+ lyso. inhibitor; see Supplementary Methods for details). Subsequently, megalin levels in cell lysates were determined by Western blotting. Detection of α-tubulin served as a loading control. (**b**) Quantification of megalin levels in control and R3192Q_1 NPCs by densitometric scanning of replicate Western blots (exemplified in panel **a**). Levels are given relative to GST-SHH-N without lysosomal inhibitors (set to 100% ± SD). Treatment with lysosomal inhibitors significantly increased levels of megalin^{R3192Q} as compared with nontreated cells (right panel). No effect of lysosomal inhibition was seen on levels of the wild-type receptor in control NPCs (left panel) (n = 4 independent experiments, 2–3 biological replicates/experiment). Statistical significance was determined using Student's *t* test. ****$P < 0.0001$.

severe bilateral myopia (+7 dioptres). His sister was diagnosed at age 9 by family screening. Her renal function was normal (estimated glomerular filtration rate: 93 ml/min per 1.73 m^2). Urine evaluation showed similar findings to her brother, including high urinary protein/creatinine ratio (2.26 mg/mg), abnormal urinary excretion of low-molecular-weight proteins (urinary beta 2 microglobulin/creatinine ratio: 1.31 mg/mg), and mild hypercalciuria (urinary calcium/creatinine ratio: 0.25 mg/mg). A small phosphate leak was also noticed (serum phosphate: 3.4 mg/dl; TmP/GFR: 2.7 mg/dl) without evidence of hyperparathyroidism (intact parathyroid hormone 31 pg/ml). No other serum or urinary abnormalities were noticed. Renal ultrasound showed normal sized kidneys (approximately 50th percentile) with discrete cortical hyperechogenicity. Her physical examination showed normal blood pressure and was significant for severe bilateral myopia (+9 dioptres), short stature (height SD: −2.13), and mild overweight (body mass index: 26.7).

Analysis of human specimen and cell lines

The study of human specimens and cell lines was approved by the Ethics Committee of Ospedale Pediatrico Bambino Gesù (approval no.: 1235_OPBG_2016). All subjects gave written informed consent before participating in this study. Generation of iPSCs was performed using the CytoTune-iPS 2.0 Sendai Reprogramming Kit. Differentiation of iPSCs to NPCs or RPTECs was performed according to published protocols[13,16] and detailed in Supplementary Methods. Differentiation into the 3 germ layers was carried out using a commercial kit according to the supplier's recommendations (Trilineage Differentiation Kit, Miltenyi Biotec, Bergisch Gladbach, Germany, No. 130-115-660). Immunodetection of megalin in renal biopsies and documentation of urinary loss of receptor ligands in spot urine of patients and control subjects shown here were performed as reported earlier.[11]

Cell studies

Studies were conducted in NPCs or RPTECs using the experimental conditions described in the respective figure legends. GST and GST-SHH-N used as ligands were affinity purified from bacterial cultures using glutathione affinity chromatography as described previously.[4] Lysozyme purified from hen egg white was obtained commercially (Abcam, Cambridge, UK, 10837059001). Experimental details for immunodetection of proteins using Western blotting or immunocytochemistry are given in the Supplementary Methods section.

Quantitative real-time polymerase chain reaction

Total RNA was extracted from cell cultures using the RNeasy Mini Kit (QIAGEN, Hilden, Germany) according to the manufacturer's instructions with an additional step of treating the RNA with RNase-free DNase I for 15 minutes at room temperature. RNA (500 ng to 1 μg) was reverse transcribed using the High Capacity RNA to cDNA Kit (Applied Biosystems, Foster City, CA). For cDNA amplification, TaqMan-Oligonucleotide probes were used with the TaqMan Gene Expression Master Mix (Applied Biosystems) on a 7900 HT Fast Real time PCR System (Thermo Fisher Scientific, Waltham, MA) and the Sequence detection system V2.4 (Thermo Fisher Scientific). Results

were analyzed using the comparative cycle threshold method normalized to *GAPDH*.[22]

Statistical analysis

All statistical analysis was performed using the GraphPad Prism 7.0 software (San Diego, CA). The applied statistical tests are indicated in the respective figure legend. Data are presented as mean ± SD. To determine the degree of colocalization between megalin and LAMP1 or GST-SHH-N, images with comparable background were taken for analysis and background correction was performed. Images were converted to 8-bit pixel images and individual cells were automatically outlined to define a region of interest. ImageJ was used to assess the Mander's colocalization coefficient, indicating the fraction of megalin colocalizing with LAMP1 or GST-SHH-N.[23]

DISCLOSURE

FE is a consultant to Otsuka Pharmaceuticals and Kiowa Kirin Pharmaceuticals. All the other authors declared no competing interests.

ACKNOWLEDGMENTS

The authors are indebted to Christine Kruse, Kristin Kampf, and Norman Krüger for expert technical assistance. The authors also acknowledge the Wellcome Trust Sanger Institute as the source of human induced pluripotent cell line HPSI1113i-wetu_2, which was generated under the human iPSC Initiative funded by a grant from the Wellcome Trust and the Medical Research Council, supported by the Wellcome Trust (WT098051) and the NIHR/Wellcome Trust Clinical Research Facility, and acknowledge Life Science Technologies Corporation as the provider of Cytotune.

SUPPLEMENTARY MATERIAL

Supplementary File (PDF)

Supplementary Methods.

Supplementary References.

Figure S1. Karyotypes of iPSC lines from patients with Donnai-Barrow syndrome.

Figure S2. Pluripotency markers and differentiation potential of iPSCs from Donnai-Barrow patients.

Figure S3. Neuroectodermal differentiation of iPSC lines from Donnai-Barrow patients.

Figure S4. Megalin^{R3192Q} expression is impaired post-transcriptionally in a second patient.

Figure S5. Generation of iPSCs genetically deficient for *LRP2*.

Figure S6. Ligand-induced decay of megalin^{R3192Q} in NPCs from a second patient.

Figure S7. Differentiation of iPSCs into renal proximal tubular epithelial-like cells.

Figure S8. Lysozyme does not induce decay of megalin^{R3192Q} in RPTECs.

Figure S9. Binding of GST-SHH-N directs megalin^{R3192Q} to lysosomes in NPCs from a second patient.

REFERENCES

1. Kantarci S, Al-Gazali L, Hill RS, et al. Mutations in LRP2, which encodes the multiligand receptor megalin, cause Donnai-Barrow and facio-oculo-acoustico-renal syndromes. *Nat Genet*. 2007;39:957–959.
2. Pober BR, Longoni M, Noonan KM. A review of Donnai-Barrow and facio-oculo-acoustico-renal (DB/FOAR) syndrome: clinical features and differential diagnosis. *Birth Defects Res A Clin Mol Teratol*. 2009;85:76–81.
3. Christ A, Christa A, Klippert J, et al. LRP2 acts as SHH clearance receptor to protect the retinal margin from mitogenic stimuli. *Dev Cell*. 2015;35:36–48.
4. Christ A, Christa A, Kur E, et al. LRP2 is an auxiliary SHH receptor required to condition the forebrain ventral midline for inductive signals. *Dev Cell*. 2012;22:268–278.
5. Cases O, Obry A, Ben-Yacoub S, et al. Impaired vitreous composition and retinal pigment epithelium function in the FoxG1::LRP2 myopic mice. *Biochim Biophys Acta Mol Basis Dis*. 2017;1863:1242–1254.
6. Verroust PJ, Birn H, Nielsen R, et al. The tandem endocytic receptors megalin and cubilin are important proteins in renal pathology. *Kidney Int*. 2002;62:745–756.
7. Christensen EI, Birn H. Megalin and cubilin: multifunctional endocytic receptors. *Nat Rev Mol Cell Biol*. 2002;3:256–266.
8. Schrauwen I, Sommen M, Claes C, et al. Broadening the phenotype of LRP2 mutations: a new mutation in LRP2 causes a predominantly ocular phenotype suggestive of Stickler syndrome. *Clin Genet*. 2014;86:282–286.
9. Anglani F, Terrin L, Brugnara M, et al. Hypercalciuria and nephrolithiasis: expanding the renal phenotype of Donnai-Barrow syndrome. *Clin Genet*. 2018;94:187–188.
10. Longoni M, Kantarci S, Donnai D, Pober BR. Donnai-Barrow Syndrome. Published August 28, 2008. Updated November 21, 2018. In: Adam MP, Ardinger HH, Pagon RA, et al., eds. *GeneReviews* [Internet]. Seattle, WA: University of Washington; 1993–2020. Available at: https://www.ncbi.nlm.nih.gov/books/NBK1878/. Accessed May 3, 2020.
11. Storm T, Tranebjaerg L, Frykholm C, et al. Renal phenotypic investigations of megalin-deficient patients: novel insights into tubular proteinuria and albumin filtration. *Nephrol Dial Transplant*. 2013;28:585–591.
12. Dachy A, Paquot F, Debray G, et al. In-depth phenotyping of a Donnai-Barrow patient helps clarify proximal tubule dysfunction. *Pediatr Nephrol*. 2015;30:1027–1031.
13. Chambers SM, Fasano CA, Papapetrou EP, et al. Highly efficient neural conversion of human ES and iPS cells by dual inhibition of SMAD signaling. *Nat Biotechnol*. 2009;27:275–280.
14. Assemat E, Chatelet F, Chandellier J, et al. Overlapping expression patterns of the multiligand endocytic receptors cubilin and megalin in the CNS, sensory organs and developing epithelia of the rodent embryo. *Gene Expr Patterns*. 2005;6:69–78.
15. McCarthy RA, Barth JL, Chintalapudi MR, et al. Megalin functions as an endocytic sonic hedgehog receptor. *J Biol Chem*. 2002;277:25660–25667.
16. Hariharan K, Stachelscheid H, Rossbach B, et al. Parallel generation of easily selectable multiple nephronal cell types from human pluripotent stem cells. *Cell Mol Life Sci*. 2019;76:179–192.
17. Leheste JR, Rolinski B, Vorum H, et al. Megalin knockout mice as an animal model of low molecular weight proteinuria. *Am J Pathol*. 1999;155:1361–1370.
18. Nykjaer A, Dragun D, Walther D, et al. An endocytic pathway essential for renal uptake and activation of the steroid 25-(OH) vitamin D3. *Cell*. 1999;96:507–515.
19. Morales CR, Zeng J, El Alfy M, et al. Epithelial trafficking of Sonic hedgehog by megalin. *J Histochem Cytochem*. 2006;54:1115–1127.
20. Hobbs HH, Brown MS, Goldstein JL. Molecular genetics of the LDL receptor gene in familial hypercholesterolemia. *Hum Mutat*. 1992;1:445–466.
21. van der Westhuyzen DR, Stein ML, Henderson HE, et al. Deletion of two growth-factor repeats from the low-density-lipoprotein receptor accelerates its degradation. *Biochem J*. 1991;277(Pt 3):677–682.
22. Schmittgen TD, Livak KJ. Analyzing real-time PCR data by the comparative C(T) method. *Nat Protoc*. 2008;3:1101–1108.
23. Dunn KW, Kamocka MM, McDonald JH. A practical guide to evaluating colocalization in biological microscopy. *Am J Physiol Cell Physiol*. 2011;300:C723–C742.